Materials Research Proceedings 28 (2023) 1739-1746 https://doi.org/10.21741/9781644902479-188

Process characteristics of constrained friction processing of AM50 magnesium alloy

DE CASTRO Camila C.[1,a *], SHEN Junjun[1,b],
DOS SANTOS Jorge F.[1,2,c] and KLUSEMANN Benjamin[1,3,d]

[1]Helmholtz Zentrum Hereon, Institute of Materials Mechanics, Solid State Joining Processes, Geesthacht, Germany

[2]Pacific Northwest National Laboratory, Richland, WA, United States

[3] Leuphana University Lüneburg, Institute for Production Technology and Systems, Lüneburg, Germany

[a]camila.castro@hereon.de, [b]junjun.shen@hereon.de, [c]jorge.dossantos@pnnl.gov, [d]benjamin.klusemann@hereon.de

Keywords: Constrained Friction Processing, Solid-State Processing, Mg Alloy, Fine Grains

Abstract. Constrained Friction Processing (CFP) is a novel solid-state technique suitable to produce rods especially from lightweight materials. The technology is particularly interesting to overcome the processing challenges associated with Mg due to its hexagonal close-packed (hcp) structure. The process is a variation of the refill friction stir spot welding (refill FSSW) technique, and is performed by plunging the rotating shoulder into the base material, which causes the material to be extruded into the cavity crated by the retraction of the rotating probe and, at the same time, being constrained by it. The complex shear and the heat generated during the process causes metallurgical transformations in the material, such as dynamic recrystallization, allowing for substantial grain refinement to micro- or even submicro- scale. In this study, real time data – torque, axial force and temperature – acquired from the process are analyzed in order to present, for the first time, a description of the CFP technique. Furthermore, the resultant features of the microstructure of a refined rod is explored.

Introduction

The demand for lightweight and environmental-friendly materials has increased over the years as the urge for reduction in greenhouse gas emissions scales [1]. In this scenario, the adoption of Mg and its alloys as structural materials is expected to increase due to their properties such as low density (1.74 g/cm³) and, thus, high strength-to-weight ratio. Nonetheless, the processing of these materials remains a challenge due to Mg's poor workability associated to the hcp crystal structure, which has a limited number of slip systems at room temperature [2].

Severe plastic deformation (SPD) techniques have been investigated for the processing of Mg alloys as means of microstructure tailoring aiming grain refinement and texture modification, which result in improvements on mechanical properties. Among those, Equal-Channel Angular Pressing (ECAP) was demonstrated to produce a refined microstructure on magnesium alloys after multiple passes, which is responsible to enhance the material ductility at moderate temperatures [3]. High-pressure Torsion (HPT) is reported to be capable of producing ultrafine microstructures Mg alloys, with an effect of doubling the strength of the base material [4].

While these techniques have been demonstrated to be able to produce fine-grained Mg and Mg alloy samples both for study of their fundamental properties and for potential applications, they may involve or even require multiple passes, considerable set up and processing times, besides potential dimensional limitations in the samples that can be produced. Most of these limitations

are alleviated or even overcome by using a newly developed technique called Constrained Friction Processing (CFP).

This friction-based technique is suitable for thermo-mechanical processing of lightweight alloys and is based on the fundamentals of the refill friction stir spot welding (refill FSSW) technique [5], but optimized for the production of extruded rods with fine or even ultrafine microstructures. CFP is performed using a 3-part toolset (a stationary clamping ring and the shoulder and probe as the rotating parts), and the processing steps are summarized in Fig. 1. Initially, the toolset reaches the surface of the plate for the clamping of the system using the set clamping force (a). Then, the rotating shoulder plunges into the base material, generating heat due to the friction and plasticizing the material. At the same time, the rotating probe is moved in the opposite direction in order to create a cavity to accommodate the plasticized material displaced by the shoulder and to constrain the material flow (b). Once the desired plunge depth is reached, the rotation of the tools stops and the shoulder is retracted to the level of the probe (c). Finally, the clamping of the plate is released and the tool system is removed, leaving a processed rod (d). The complete process time takes only few seconds depending on the plunge depth, what qualifies the CFP as a fast and simple way to obtain rods with refined microstructure.

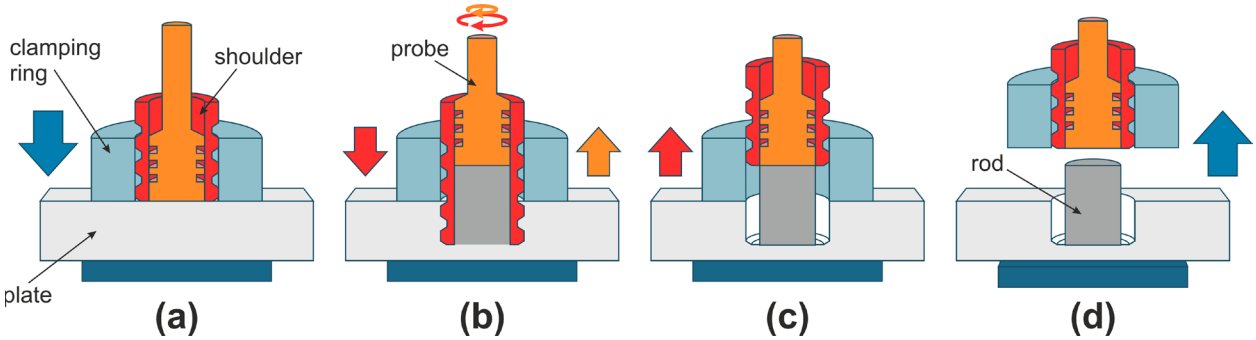

Fig. 1. Schematic representation of CFP: (a) clamping of the plate, (b) plunging, (c) shoulder retraction and (d) releasing steps.

The present study analyzes CFP characteristics in terms of torque, axial force and the temperature evolution in order to better understand the process and enable its further development. Typical CFP rods were processed using as-cast AM50 as base material, and information such as torque and axial force were recorded for each tool part, as well as the process temperature, which was measured using a thermocouple placed at the base of the processed rod. Finally, the microstructure of a typical rod is analyzed in order to demonstrate the potential of CFP on grain refinement.

Materials and Methods

The base material selected in this study is an as-cast AM50 magnesium alloy, obtained via permanent mold casting, as described by Elsayed et al. [6]. The as-cast material features a microstructure with typical dendritic grains (with grain sizes in terms of average diameter varying from 457 to 1023 μm), eutectic β-Mg17Al12 and secondary Al-Mn phases.

In this study, CFP rods were produced using a refill FSSW machine (RPS 200, Harms-Wende GmbH) operated in position control mode. Both axial and rotational movement of each tool part is actuated using individual transducers. The axial forces produced during the process on the rotating parts of the tool can be measured using four shear pancake load cells for each component. Furthermore, the torque produced by the probe and the shoulder is measured using a system consisting of a lever arm attached to the motor spindle that transmits the force to the load cell, also a shear pancake type. A schematic representation of the toolset is given in Fig. 2, which consists

of a molybdenum-vanadium alloyed hot-work tool-steel clamping ring (⌀17 mm) and probe (⌀6 mm), and a G40 tungsten carbide shoulder (⌀9 mm), resulting in an extrusion ratio of 2.25. For the experiment, a total of two samples were produced: one for the torque and axial force measurements, which was subsequently submitted to the microstructural, and one for the acquisition of the temperature evolution. In all cases, the rotation speed (RS) for both shoulder and probe was set as 1800 rpm, combined with a shoulder plunge speed (PS) of 1 mm/s at a constant clamping ring force of 12 kN. The plunge depth (PD) was set as 3.00 mm, resulting in a rod with a total length of 6.75 mm. The process parameters were selected based on preliminary experiments aiming the determination of the suitable processing window. The workpiece used for the CFP with dimensions of 100 x 25 x 6 mm³ was fixed to the stainless steel backing plate attached to the working table, ensuring the stability of the system during the process. No post-processing cooling was used in this study, whereby the produced rods were air cooled.

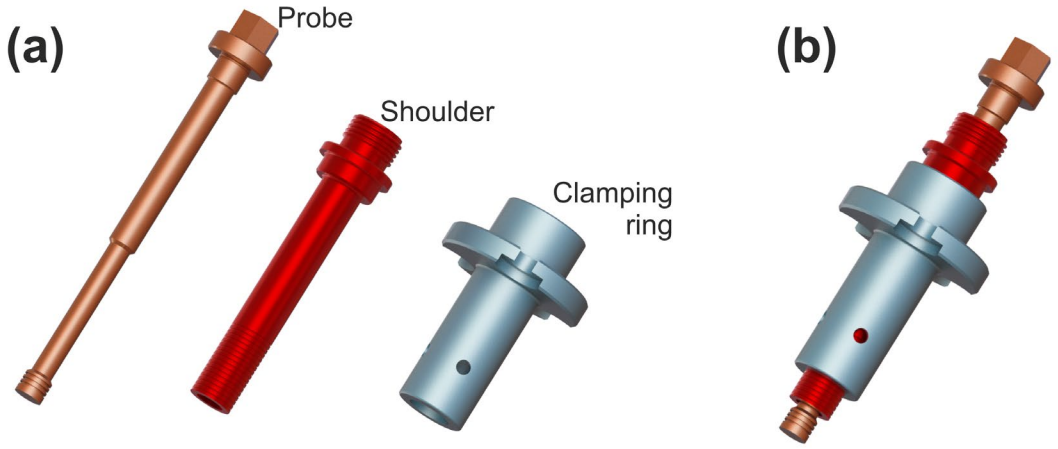

Fig. 2. Schematic representation of the toolset: (a) probe, shoulder and clamping ring, and (b) toolset assembly.

The temperature evolution during CFP was measured using a K-type thermocouple with an acquisition frequency of 50 Hz. The precision of the used thermocouple is ± 2.2 °C or ± 0.75% of the measured temperature, whichever is greater [7]. For this measurement, a 2.5 mm long, 0.6 mm diameter hole was drilled on the back of the workpiece, in a concentric position in relation to the tools. Therefore, the temperature was measured at a point 0.5 mm away from the root of the rod.

For the microstructural analysis, the rod was embedded in acrylic resin, grounded to #4000 Si C foil until the cross-section was reached, and mechanically polished to 0.2-µm water-free colloidal silica suspension. In order to reveal the rod's microstructure, the sample was etched by immersion for 15 s using an acetic-picric solution (180 mL ethanol, 20 mL distilled water, 7.5 mL acetic acid, 4 g picric acid). The metallographic analysis was performed using a VHX-6000 digital microscope. Micrographs were acquired using a Leica DMi8 microscope, where the grain size (d), i.e. average grain diameter, was measured according to ASTM E 112 (grain boundary intersection count method) [8] using the ImageJ 1.52a software [9].

Results and Discussion

Process Characteristics of CFP.

The position of the rotating tools (shoulder and probe) during CFP was recorded and is depicted in Fig. 3(a), along with the RS data. The process starts at t = 0 s, when the toolset just reached the surface of the plate, and the set clamping ring force was applied. In the plots, the tool plunge is indicated with positive values on the *y-axis*, while the retraction of the probe corresponds to negative values. With a set shoulder and probe RS of 1800 rpm, the shoulder starts to plunge the

Materials Research Proceedings 28 (2023) 1739-1746 https://doi.org/10.21741/9781644902479-188

material at a PS of 1.00 mm/s. For this processing route, the displacement of the rotating tools was set to follow a sine profile. The average volume of extruded material is 35.34 mm³/s. In order to constrain this volume of material without imposing any compression, the probe retraction speed is set as 1.25 mm/s, resulting in a total displacement of 3.75 mm at the end of the process.

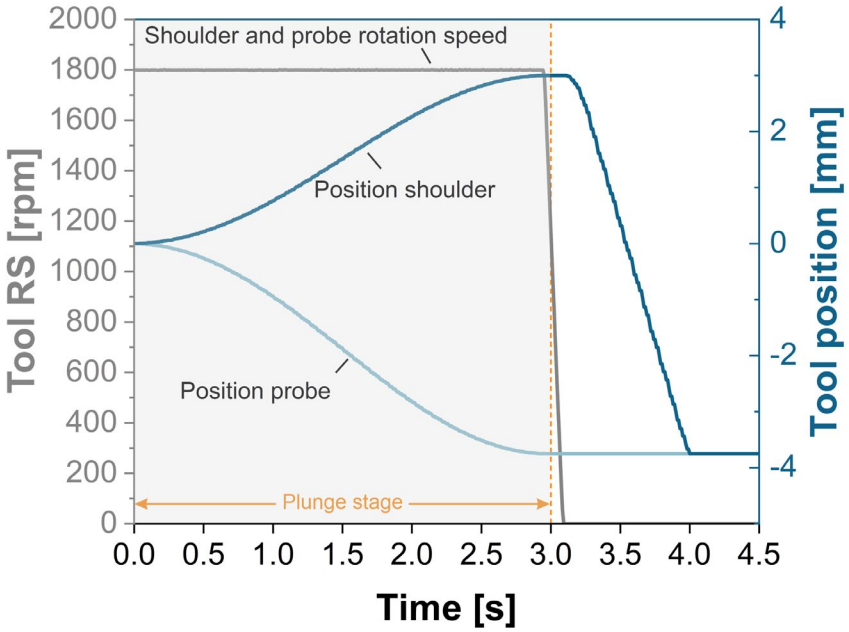

Fig. 3. Position and rotation speed (RS) data acquired for probe and shoulder during CFP.

The torque and axial forces for the probe and the shoulder are presented in Fig. 4. The axial forces correspond to the resistance of the material to the extrusion component of the CFP. For a better understanding of the mechanical efforts associated to the process, it is important to read the results of the actual CFP presented in Fig. 4 (a) along with the plots of the CFP performed without plunging into the workpiece, Fig. 4 (b), that represents the forces and torque related to the friction between the machine components and tool parts. In terms of axial forces, the effect of friction is negligible. The actual CFP axial forces measurement indicates a maximum force during the plunging of around 5.47 kN for the shoulder at t = 0.98 s. For the probe, the maximum axial force (1.66 kN) was measured at the beginning of the process. This likely corresponds to the reaction force to the material stuck between shoulder and probe remaining from the previous processing operation, since the material is not yet plasticized at this moment. Combined with the stuck material, this reaction force is also related to the displaced material produced on the probe due to the beginning of the shoulder plunge.

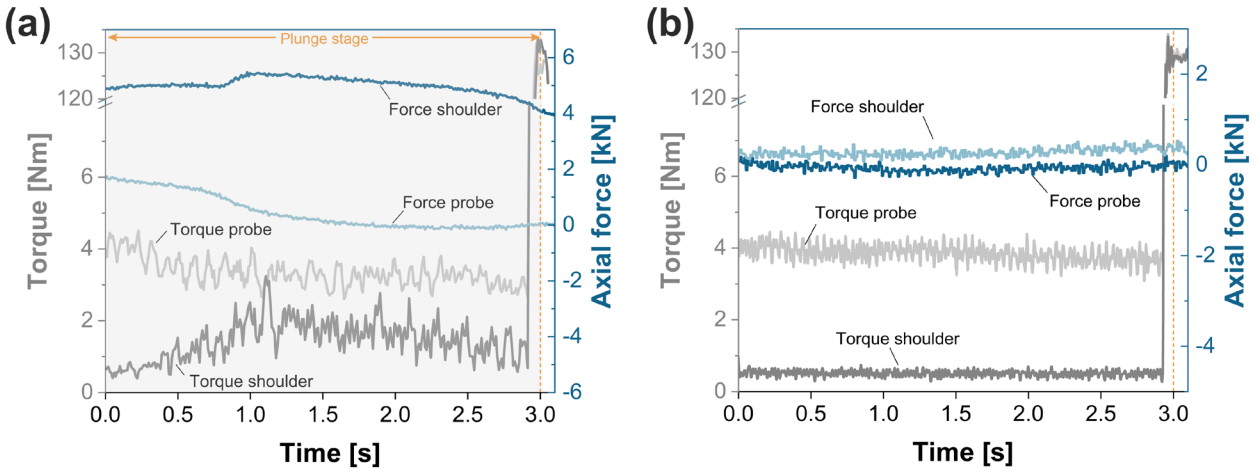

Fig. 4. Torque and axial force data acquired for probe and shoulder during CFP (a) on AM50 workpiece. (b) Measured torques and axial forces due to internal friction, without plunging into the workpiece.

The torque measurements during the CFP indicate the resistance of the material to be stirred due to the rotation of the tool, and are especially interesting for the shoulder. This is attributed to the negligible contribution of the probe to the torque, evidenced by Fig. 4, which shows an average of around 4 Nm. This is somehow expected, since the only contact between probe and material is on its lower surface and the shoulder and probe rotate at the same speed, generating a material flow that doesn't impose significant stresses at this surface. For the shoulder, the torque increases from the beginning of the process until it reaches its peak value of 3.20 Nm around t = 1.10 s. This is an indication of the obvious increase in the resistance of the material to the rotation movement as the shoulder plunging progressively increases. From this peak point on, the torque continuously decreases until the end of the process. It is interesting to point out that the peak values for torque and axial force are reached at the same time, indicating that at this point the material reaches the temperature and shearing conditions leading to plasticization.

As the shoulder approaches the set PD, the control system of the machine starts to drastically reduce the toolset RS to zero at t = 2.94 s for 0.15 s, resulting in a deceleration of 12032 rpm/s (Fig. 3). The deceleration of the tool results in a drastic increase of the torque up to 132 Nm for both probe and shoulder. The process then finishes with the shoulder moved upwards to the same position as the probe (y = -3.75), and releasing the clamping ring force, leaving the processed rod.

The analysis of the temperature measurements, depicted in Fig. 5, indicates that the peak values of torque and axial force for the shoulder occur at around 205°C (478 K). This corresponds to 52% of the AM50 melting temperature, according to differential scanning calorimetry (DSC) measurements reported by Kasprzak et al. [10], i.e. solidus and liquidus temperature of 434°C (707 K) and 640°C (913 K), respectively. Another aspect observed in Fig. 5 is that the peak temperature produced during the plunge stage of the process, Fig. 1(b), measured as 468°C (741 K), is 34°C above the solidus temperature of AM50 alloy and corresponds to 81% of the AM50 liquidus temperature.

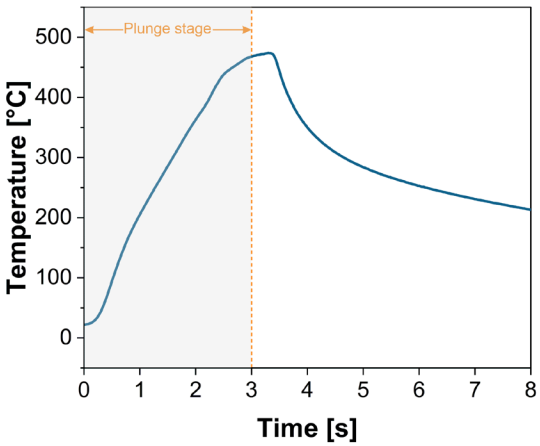

Fig. 5. Temperature evolution during CFP, measured via thermocouple placed at the rod's root.

Microstructure produced by CFP.

The microstructures of the base material and of the rod produced from the conditions presented are depicted in Fig. 6. The comparison of the rod with the surrounding base material indicates a strongly refined microstructure, with average *d* of around 7.7 ± 1.9 µm. This represents a reduction to around 1:96 in comparison to the base material.

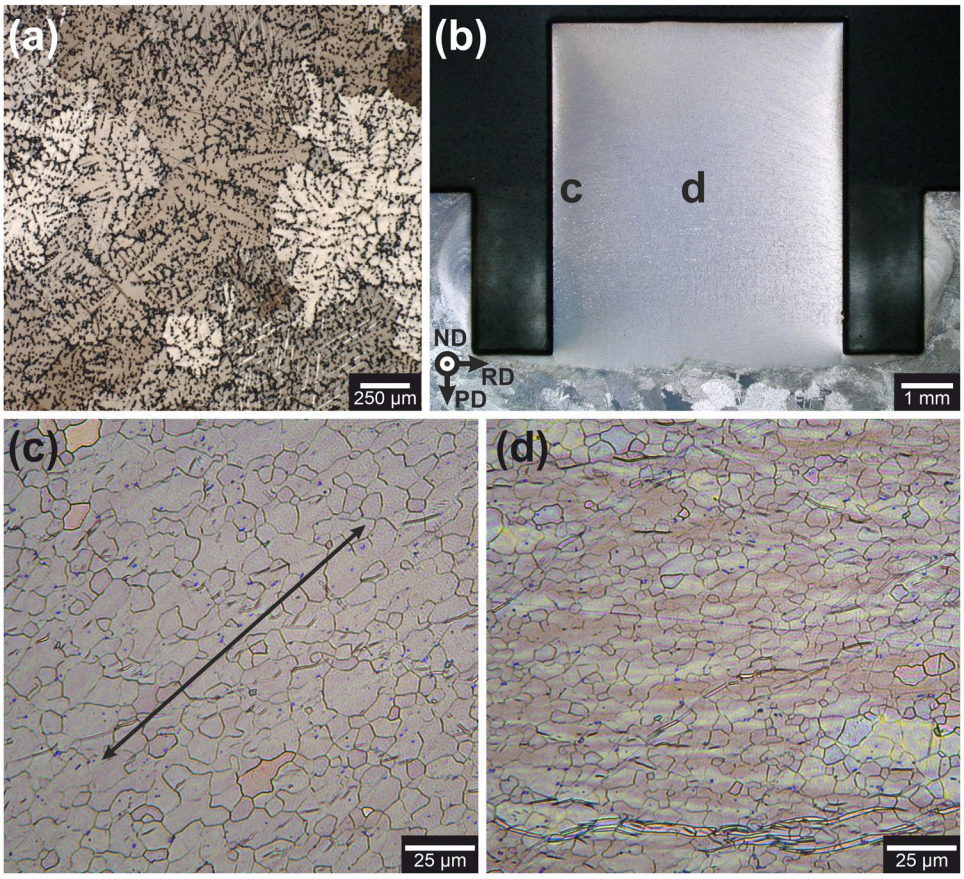

Fig. 6. Micrographs of (a) as-cast AM50 base material, (b) macrostructure of a rod produced by CFP and (c) and (d) micrographs of two selected regions of the rod.

The microstructure of a produced rod varies along the plunge direction (PD) as well as in the radial direction (RD). Two examples of microstructures are depicted in Fig. 6(c) and (d). Along the PD, it is possible to observe a refined and equiaxed microstructure with $d = 8.2 \pm 1.1$ µm. Although the grain structure along the PD is similar for every position, there is a variation in d due to the varying stirring conditions and distinct thermal histories as a function of the height. At the bottom of the rod, the average measured d is considerably smaller than the other positions of the rod, 5.4 ± 0.5 µm, while the average d at the top of the rod is 9.0 ± 0.7 µm.

Along the RD of the rod, less remarkable differences on d are observed, e.g., at the border (9.0 ± 1.8 µm) (c) and at the center (8.2 ± 1.1 µm) (d) of the rod. However, the examination of the grain structure at these two positions indicates some deformation of the grains along the direction of around 47° // PD. This may be attributed to the material flow conditions during CFP, described by Shen et al. [11] as a spiral curve similar to a conical compression spring, and developed layer by layer during the refilling stage of the refill FSSW, which is analogous to CFP.

Summary

In the present study, CFP was introduced and its characteristics were investigated in terms of torque, axial force and temperature evolution during the process. Furthermore, the microstructure of a typical AM50 rod produced via the novel CFP was analyzed. The main findings are summarized below:

- Although the probe plays an important role on the constraint of the material flow, the torque evolution during the process is negligible for this tool part. For the axial force, a peak value of 1.66 kN is found at the beginning of the process and is progressively reduced to roughly zero.
- The data acquired for the shoulder indicates peak values of torque of 3.2 Nm at t = 1.1 s and axial force of 5.47 kN at t = 0.98 s, i.e., roughly at the same moment. In this time interval, the temperature measured at the bottom of the rod reads around 200 °C, suggesting that the temperature of plasticization of AM50 during CFP is at least 52% of AM50's melting temperature.
- The produced microstructure has an average d of around 7.7 ± 1.9 µm, which represents a reduction of the initial as-cast base material of around 1:96. It is interesting to point out that this remarkable d reduction was obtained using a simple process setup in only 3 s of processing time, indicating suitable upscale potential of CFP.

References

[1] European Environment Agency, Greenhouse gas emissions from transport in Europe. Retrieved from https://www.eea.europa.eu/data-and-maps/indicators/transport-emissions-of-greenhouse-gases-7

[2] Z. Wu, R. Ahmad, B. Yin, S. Sandlöbes, W.A. Curtin, Mechanist origin and predicion of enhanced ductility in magnesium alloys, Science 359 (2018) 447-452. https://doi.org/10.1126/science.aap8716

[3] R.B. Figueiredo, T.G. Langdon, Grain refinement and mechanical behavior of a magnesium alloy processed by ECAP, J. Mater. Sci. 45 (2010) 4827–4836. https://doi.org/10.1007/s10853-010-4589-y

[4] R.B. Figueiredo, M.T.P. Aguilar, P.R. Cetlin, T.G. Langdon, Deformation heterogeneity on the cross-sectional planes of a magnesium alloy processed by high-pressure torsion, Metall. Mater. Trans. A Phys. Metall. Mater. Sci. 42 (2011) 3013-3021. https://doi.org/10.1007/s11661-011-0609-z

[5] C. Schilling, J.F. Dos Santos, Method and device for linking at least two adjoining work pieces by friction welding, European Patent Office. EP1230062 (2000)

[6] F.R. Elsayed, N. Hort, M.A. Salgado-Ordorica, K. Kainer, Magnesium permanent mold Castings optimization, Mater. Sci. Forum. 690 (2011) 65-68. https://doi.org/10.4028/www.scientific.net/MSF.690.65
[7] ASTM International, ASTM E230 - Standard Specification for Temperature-Electromotive Force (emf) Tables for Standardized Thermocouples, (2017). https://doi.org/10.1520/E0230_E0230M-17
[8] ASTM International, ASTM E112 - Standard Test Methods for Determining Average Grain Size, (2021). https://doi.org/10.1520/E0112-13R21
[9] C.A. Schneider, W.S. Rasband, K.W. Eliceiri, NIH Image to ImageJ: 25 years of image analysis, Nat. Methods. 9 (2012) 671–675. https://doi.org/10.1038/nmeth.2089
[10] W. Kasprzak, J.H. Sokolowski, M. Sahoo, L. Dobrzanski, Thermal and structural characteristics of the AM50 magnesium alloy, J. Achieve. Mater. Manuf. Eng. 28 (2008) 131-138.
[11] J. Shen, S.B.M. Lage, U.F.H. Suhuddin, C. Bolfarini, J.F. dos Santos, Texture Development and Material Flow Behavior During Refill Friction Stir Spot Welding of AlMgSc, Metall. Mater. Trans. A Phys. Metall. Mater. Sci. 49 (2018) 241-254. https://doi.org/10.1007/s11661-017-4381-6